CHEMISTRY OF MATERIALS

pubs.acs.org/cm

Article

Lockable Multiple Twisting in Donor−Acceptor Molecules for Emergent Crystalline Structures and Optical Properties

Lishan Sun,[+] Chenglong Liao,[+] Zihua Zhu, Yangyang Ren, Ran Duan, Hongwei Ji, Ling Zang,* Yanke Che,* and Jincai Zhao

Cite This: *Chem. Mater.* 2025, 37, 1570−1577

Read Online

ACCESS | Metrics & More | Article Recommendations | Supporting Information

ABSTRACT: In comparison to incorporating different functional groups into rigid molecules to generate diverse interaction competitions, achieving lockable multiple twisting conformations in the molecular backbone can provide a similar capability. This approach also helps streamline the synthesis process and reduces the likelihood of unintentional property impairments. However, this strategy remains largely unexplored in small molecules. Here, we report the development of a donor−acceptor (D−A) molecule with a D−D−A−D−D backbone structure and sophisticated side-chain design that enables lockable multiple twisting conformations in its molecular backbone. Through heteroseeded self-assembly, orange-emitting two-dimensional (2D) platelets can be formed. These platelets consist of a unique D-D-A-D-D conformer with a benzothiadiazole group and neighboring fluorene groups arranged in almost the same plane but with a significant twisting relative to the next attached fluorene groups. The resulting 2D platelets exhibit a pronounced redshift in their optical properties compared to the monomer in solution, along with a high fluorescence quantum yield of approximately 73%. Furthermore, this molecule can adopt two intertwined conformations with large twisting angles to form one-dimensional (1D) microribbons, which emit green light. The packing of these two conformations results in slightly red-shifted optical spectra compared to the monomer in solution and a high fluorescence quantum yield of around 87%.

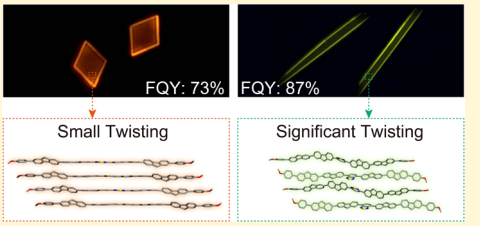

1. INTRODUCTION

The incorporation of various intermolecular interactions can result in the emergence of different interaction competitions, ultimately giving rise to aggregates with a range of energy well depths. In specific solvent environments, some aggregates determined by certain intermolecular interactions may adopt one molecular packing and then evolve into a different packing in a more stable energy state (or interactions).[1−22] This approach has been effectively utilized in a variety of molecular systems with a rigid backbone, resulting in diverse morphologies with distinct properties.[1−15,17−20] Despite its effectiveness, there are drawbacks associated with this method. One downside is the complexity and tedium involved in synthesizing building blocks with various functional groups for multiple interactions. Additionally, the inclusion of certain groups within a molecule that are intended for specific interactions can be challenging to anticipate as beneficial for preferred morphologies and favorable properties. One recent example is donor−acceptor (D−A) fluorophores with benzimidazole end groups, which enable the formation of hydrogen bonds with alcohols.[23,24] While crucial for creating diverse two-dimensional (2D) shapes, the functional groups significantly reduce photostability.

Instead of introducing different functional groups to achieve various intermolecular interactions, an alternative method could be utilizing molecules that have lockable twist in their molecular backbone to generate diverse molecular organizations and consequently, emergent properties. By accessing multiple molecular backbone conformations for different intermolecular interactions, this strategy can result in the creation of diverse morphologies and properties, while also streamlining the synthesis process and reducing the likelihood of unforeseen property impairments. Despite its potential, this method remains largely unexplored in small molecules, possibly due to the limited availability of flexible molecule candidates and effective techniques for achieving the lockable specific twisting conformations. Recently, heteroseeded self-assembly has demonstrated the capability to guide polymers[25−27] or small molecules[18,28−31] to grow epitaxially on the heteroseeds, leading to the creation of distinct molecular packing that differs from what would form on their own. These findings motivated us to explore the potential of utilizing the heteroseeding method to guide molecules with twisting flexibility, producing specific structures alongside what would naturally form.

Received: November 18, 2024
Revised: January 28, 2025
Accepted: January 29, 2025
Published: February 4, 2025

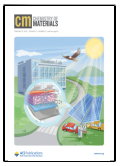

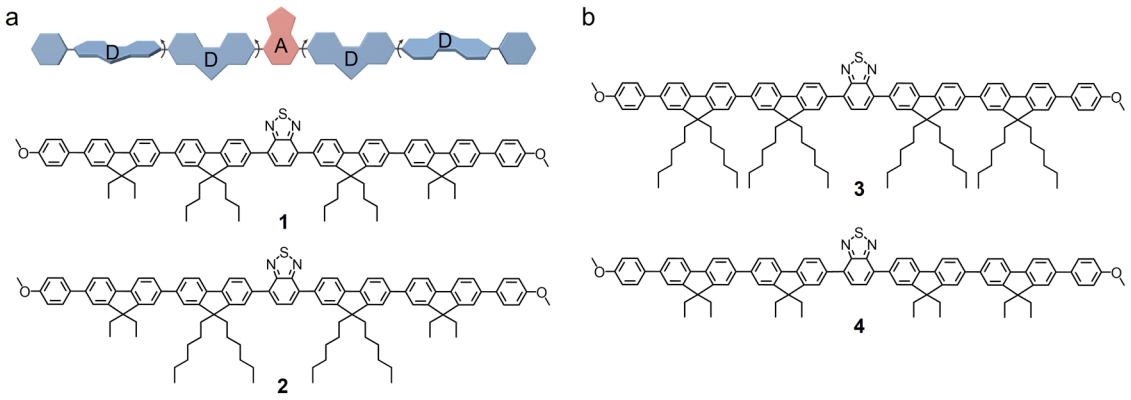

Figure 1. (a) Schematic diagram showing the twisting of the molecular backbone of molecules **1**,**2**. (b) Molecular structures of molecules **3**,**4**.

We recently observed that a D−A molecule (molecule **2**, Figure 1a) displayed multiple twisting conformations in its molecular backbone, but with minimal variation across all conformers.[15] This restriction in variation led to the formation of aggregates confined to 2D shapes. This observation prompted us to explore lockable multiple conformations with substantial twisting variation in the molecular backbone, leading to the formation of aggregates with distinct morphology and optical characteristics. To achieve this, we synthesized the D−A molecule **1** in this study, which has a D−D−A−D−D backbone structure and alkyl side chains of varying lengths on the two fluorene units (Figure 1a). We demonstrate that molecule **1** has the ability to form two different types of single-crystalline structures, specifically 2D platelets and 1D microribbons, as a result of the different twisting conformations in the molecular backbone. Upon using heteroseeded self-assembly, diamond-like 2D platelets can be grown exclusively. Single-crystal analysis reveals that the twisting angles between the benzothiadiazole group and its neighboring fluorene groups are very small (around 2°), while the twisting angles between the fluorene groups are significant (around 30°). The former leads to a significant redshift in both absorption and fluorescence spectra of the conformer compared to the monomer in solution, while the latter hinders a strong electron coupling between neighboring molecules. Consequently, the resulting diamond-like 2D platelets display a high emission efficiency of around 73% and a substantial red-shifted emission. Moreover, molecule **1** has the capability to form 1D microribbons. These microribbons consist of two distinct conformers of molecule **1**, each exhibiting significant twisting between the A and D groups. The intertwining of these conformers within the crystalline structure results in the enhanced stability of the 1D microribbons. Additionally, the presence of these large twisting conformers contributes to the high emission efficiency of approximately 87% and slightly red-shifted emission observed in the 1D microribbons compared to the monomer in solution.

2. EXPERIMENTAL SECTION

2.1. Synthesis of Molecules 1−4. *2.1.1. Synthesis of Molecule 1.* Detailed synthesis and characterization are included in the Supporting Information. ^{1}H NMR (400 MHz, Chloroform-d, ppm) δ 8.08 (d, J = 7.9 Hz, 2H), 8.00 (s, 2H), 7.92 (d, J = 6.8 Hz, 4H), 7.87 (s, 1H), 7.85 (s, 1H), 7.83 (s, 1H), 7.80 (d, J = 2.9 Hz, 2H), 7.78 (s, 1H), 7.73−7.67 (m, 6H), 7.65 (d, J = 3.4 Hz, 4H), 7.62 (s, 2H), 7.58 (s, 1H), 7.56 (s, 1H), 7.55 (s, 2H), 7.02 (d, J = 8.8 Hz, 4H), 3.89 (s, 6H), 2.16 (q, J = 6.9 Hz, 16H), 1.17 (p, J = 7.3 Hz, 8H), 0.86 (p, J = 7.9, 7.2 Hz, 8H), 0.76 (t, J = 7.3 Hz, 12H), 0.47 (t, J = 7.3 Hz, 12H) (Figure S1). MALDI-TOF-MS: (m/z) = 1341.572 (Figure S2).

2.1.2. Synthesis of Molecule 2. Molecule **2** was synthesized by following the previously reported method.[29] ^{1}H NMR (400 MHz, Chloroform-d, ppm) δ 8.06 (d, J = 7.8 Hz, 2H), 8.00 (s, 2H), 7.86 (m, 10H), 7.61 (m, 16H), 7.02 (d, J = 8.2 Hz, 4H), 3.89 (s, 6H), 2.16 (d, J = 10.1 Hz, 16H), 1.23−1.02 (m, 24H), 0.87 (d, J = 9.0 Hz, 8H), 0.78 (t, J = 6.6 Hz, 12H), 0.46 (t, J = 7.3 Hz, 12H) (Figure S3). MALDI-TOF-MS: (m/z) = 1454.26 (Figure S4).

2.1.3. Synthesis of Molecule 3. Detailed synthesis and characterization are included in the Supporting Information. ^{1}H NMR (400 MHz, Chloroform-d, ppm) δ 8.06 (d, J = 7.9 Hz), 8.01, 7.92 (d, J = 5.4 Hz), 7.87 (d, J = 7.8 Hz), 7.79 (d, J = 10.6, 7.8 Hz), 7.71−7.61 (m), 7.56 (d, J = 10.3 Hz), 7.03 (d, J = 8.8 Hz), 3.89, 2.11 (d, J = 18.9, 13.4, 6.5 Hz), 1.57, 1.13 (dd, J = 12.5, 4.3 Hz), 0.78 (q, J = 6.8 Hz) (Figure S5). MALDI-TOF-MS: (m/z) = 1678.196 (Figure S6).

2.1.4. Synthesis of Molecule 4. Detailed synthesis and characterization are included in the Supporting Information. ^{1}H NMR (400 MHz, Chloroform- d, ppm) δ 8.07 (d, J = 8.1 Hz, 2H), 8.01 (s, 2H), 7.93 (d, J = 4.9 Hz, 4H), 7.87 (d, J = 7.6 Hz, 2H), 7.80 (t, J = 8.2 Hz, 4H), 7.76−7.60 (m, 12H), 7.59−7.52 (m, 4H), 7.02 (d, J = 8.3 Hz, 4H), 3.88 (s, 6H), 2.26−2.09 (m, 16H), 0.54 (t, J = 7.2 Hz, 12H), 0.46 (t, J = 7.3 Hz, 12H) (Figure S7). MALDI-TOF-MS: (m/z) = 1229.022 (Figure S8).

2.2. Fabrication of Different Aggregates. *2.2.1. Fabrication of Aggregates from 1 via Conventional Self-Assembly.* Two distinct types of aggregates, as shown in Figure S9 below, were formed simultaneously after injecting 0.1 mL of a chloroform solution of **1** (0.5 mg/mL) into 1 mL of acetonitrile in a 4 mL vial and aging the mixture at 25 °C for 24 h.

2.2.2. Preparation of Orange-Emitting 2D Platelets Using the Heteroseeding Method. The heteroseeds of **2** were made using the method that had been previously described.[29] Specifically, the hexagonal platelets of **2** were first generated by injecting 1 mL of acetonitrile into 0.2 mL of a chloroform solution of **2** (0.5 mg/mL) in a 4 mL vial. The mixture was then allowed to age at 25 °C for 40 h. Following the removal of the supernatant from the hexagonal platelets suspension, 2 mL of acetonitrile was added. The resulting solution containing the platelets was then subjected to sonication at −35 °C for 5 min to obtain the seeds (0.05 mg/mL). By adding varying volumes (0.1, 0.04, 0.02, and 0.01 mL) of an acetonitrile solution containing the seeds of **2** (0.05 mg/mL) to 1.1 mL of the supersaturated solution of **1** (0.01 mg/mL) in chloroform/acetonitrile mixtures (v/v, 1/10) in a vial and aging at 25 °C for 30 min, orange-emitting 2D platelets with controlled sizes were successfully fabricated. The morphology of the orange-emitting 2D platelets of **1** was continuously monitored for several additional months.

2.2.3. Preparation of Green-Emitting 1D Microribbons Using the Homoseeding Method. The green-emitting 1D microribbons of **1** were first generated by injecting 2 mL of acetonitrile into 0.2 mL of a chloroform solution of **1** (0.5 mg/mL) in a 4 mL vial. The mixture was then allowed to age at 25 °C for 9 days. Following the removal of

https://doi.org/10.1021/acs.chemmater.4c03183
Chem. Mater. 2025, 37, 1570−1577

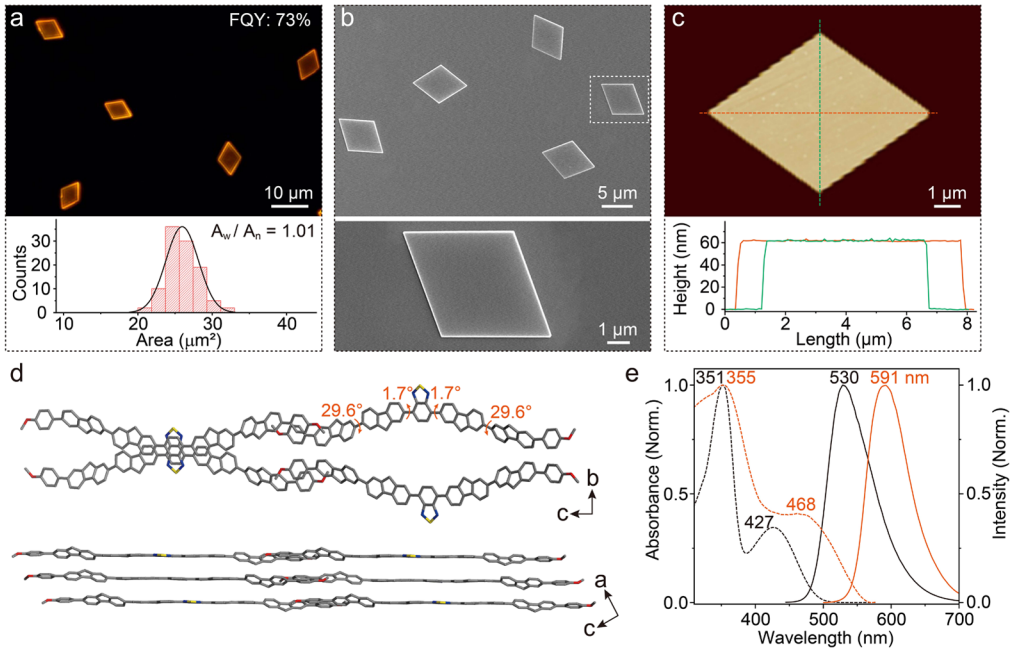

Figure 2. (a) Fluorescence-mode optical image and statistical histogram of the area dispersity of the orange-emitting 2D platelets of **1** at a molecule-to-seed mass ratio of 5:1, Aw = 26.2 μm^2, An = 26.0 μm^2, Aw/An = 1.01. (b) SEM images of the orange-emitting 2D platelets of **1**. (c) AFM height image and corresponding height profiles of an orange-emitting 2D platelet of **1**. (d) Single-crystal structure of the orange-emitting 2D platelet showing the specific conformation of molecule **1**. (e) UV−vis absorption (dashed) and fluorescence spectra (solid) of molecule **1** (6 μM) in toluene (black) and the orange-emitting 2D platelets of **1** drop-cast on a glass slide (orange).

the supernatant from the microribbon suspension, 2 mL of acetonitrile was added. The resulting solution containing the microribbons was then subjected to sonication at −35 °C for 5 min to obtain the seeds of **1** (0.05 mg/mL). By adding varying volumes (0.1, 0.04, 0.025, and 0.015 mL) of an acetonitrile solution containing the seeds of **1** (0.05 mg/mL) to 1.1 mL of the supersaturated solution of **1** (0.01 mg/mL) in chloroform/acetonitrile mixtures (v/v, 1/10) in a vial and aging at 25 °C for 30 min, the green-emitting 1D microribbons with controlled sizes were successfully fabricated. The morphology of the green-emitting 1D microribbons of **1** was continuously monitored for several additional months.

2.2.4. Growth of Bulk 2D Platelets and 1D Microribbon Crystals of 1 for Single-Crystal Analysis. The bulk orange-emitting 2D platelets with the sizes of over 50 μm in each dimension were prepared by adding **1** μL of an acetonitrile solution of seeds of **2** (0.0005 mg/mL) into 3.6 mL of a solution containing 0.01 mg/mL of **1** in a chloroform/acetonitrile mixture (v/v: 1/5) and then aging at 25 °C for 3 days. The bulk green-emitting 1D microribbons, with sizes of over 50 μm in each dimension, were prepared by combining 1 μL of an acetonitrile solution of seeds of **1** (0.0005 mg/mL) with 3.6 mL of a solution containing 0.01 mg/mL of **1** in a chloroform/acetonitrile mixture (v/v: 1/5) and then allowing it to age at 25 °C for 3 days.

2.2.5. Preparation of Aggregates from 3 and 4. Using a conventional self-assembly approach, aggregates of **3** were generated by injecting 0.1 mL of a chloroform solution containing **3** (0.5 mg/mL) into 1 mL of acetonitrile in a 4 mL vial. The solution was then aged at 25 °C for 24 h. To fabricate aggregates of **3** using a heteroseeding method, 0.1 mL of heteroseeds of **2** (0.05 mg/mL) in acetonitrile were added to a supersaturated solution of **3** (0.01 mg/mL) in a mixture of chloroform and acetonitrile (1.1 mL, v/v, 1/10) in a 4 mL vial, followed by aging at 25 °C for 24 h. The morphology of the aggregates of **3**, formed using both methods, was monitored over the course of several additional months. Using a conventional self-assembly approach, aggregates of **4** were generated by injecting 0.1 mL of a chloroform solution containing **4** (0.5 mg/mL) into 1 mL of acetonitrile in a 4 mL vial. The solution was then aged at 25 °C for 24 h. To fabricate aggregates of **4** using a heteroseeding method, 0.1 mL of heteroseeds of **2** (0.05 mg/mL) in acetonitrile were added to a supersaturated solution of **4** (0.01 mg/mL) in a mixture of chloroform and acetonitrile (1.1 mL, v/v, 1/10) in a 4 mL vial, followed by aging at 25 °C for 24 h. The morphology of the aggregates of **4**, formed using both methods, was monitored for several additional months.

2.3. Property Characterizations. Fluorescence-mode optical microscopic images were captured using an inverted fluorescence microscope equipped with a standard CCD detector (Olympus IX71), in which the samples were excited by a 365 nm ultraviolet LED light. The solution containing suspending assemblies was drop-cast onto glass substrates to prepare samples for fluorescence images. Scanning electron microscopy (SEM) images were acquired with a Hitachi S-8010 and TESCAN MI-RA LMS field-emission microscope. Atomic force microscopy (AFM) images were obtained using a Bruker Dimension Icon atomic force microscope. AFM samples were prepared by drop-casting suspending aggregates onto thin glass slides from the solution. Powder X-ray diffraction (XRD) measurements were performed on a PANalytical X'Pert PRO instrument (40 kV, 200 mA). Absorption spectra were obtained on a Hitachi U-3900 spectrometer. Fluorescence spectra were obtained on a Hitachi F-7000 fluorometer. Fluorescence quantum yields (FQYs) of molecule **1**−**4** in toluene (6 μM) and their aggregates were determined by using a Hamamatsu Absolute PL Quantum Yield spectrometer C11247 coupled with an integrating sphere. Excitation wavelengths ranging from 330 to 450 nm with an interval of 10 nm were utilized. The fluorescence lifetime of molecules **1**−**4** in toluene (6 μM) and their aggregates were determined using a time-resolved photoluminescence setup (LifeSpec II, Edinburgh Instruments), with a 365 nm pulsed laser serving as the excitation source. Selected area electron diffraction (SAED) patterns of the 2D platelets and 1D microribbons were acquired using JEOL 2100 with an electron beam energy of 120 kV. Single-crystal X-ray diffraction (SCXRD) measurements were conducted with a Rigaku XtaLAB PRO 007HF diffractometer, utilizing graphite monochromatized Mo Kα (λ = 0.71073 Å) radiation in the ω scan mode. Single-crystal structures were determined using an intrinsic phasing with SHELXT and refined by full-matrix least-squares on F^2 using SHELXL-2014. Density

https://doi.org/10.1021/acs.chemmater.4c03183
Chem. Mater. 2025, 37, 1570−1577

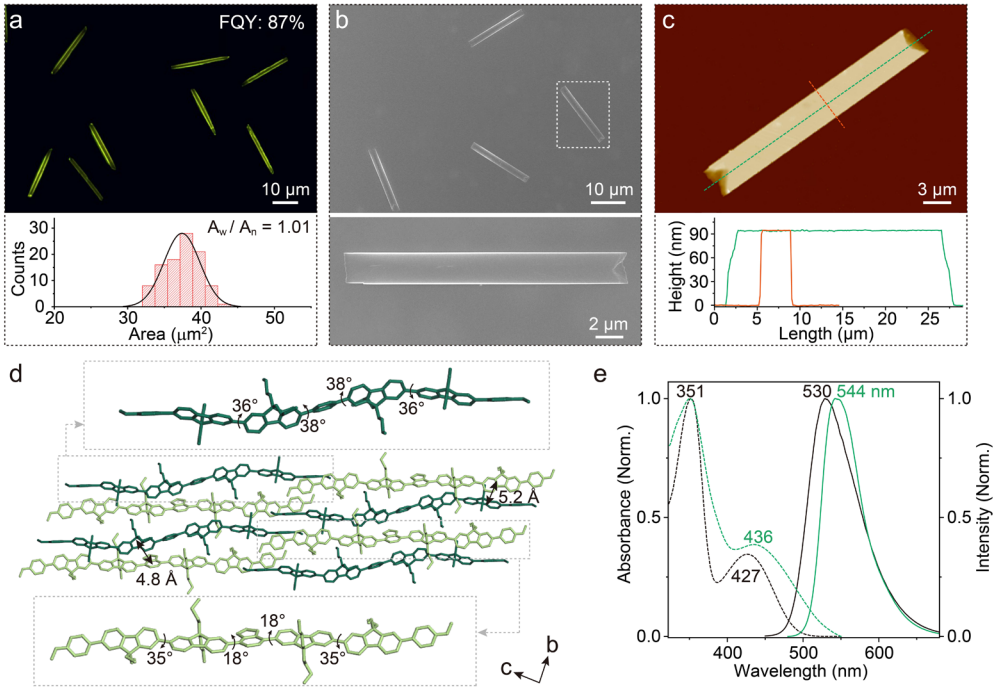

Figure 3. (a) Fluorescence-mode optical image and statistical histogram of the area dispersities of the green-emitting 1D microribbons of **1** at a mass ratio of the molecule-to-seed of 5:1, Aw = 37.4 μm^2, An = 37.6 μm^2, Aw/An = 1.01. (b) SEM images of the 1D microribbons of **1**. (c) AFM height image and corresponding height profiles of a 1D microribbon of **1**. (d) Single-crystal structure of the green-emitting 1D microribbons showing molecule **1** adopted the two different twisting conformations adopted by molecule **1**. (e) UV−vis absorption (dashed) and fluorescence spectra (solid) of molecule **1** (6 μM) in toluene (black) and the green-emitting 1D microribbons drop-cast on a glass slide (green).

functional theory (DFT) calculations were performed at the B3LYP/6-31g(d,p) level using the Gaussian 09 package. The seeds were prepared by sonication with a commercial Scientz-IID ultrasonic homogenizer operating at a power of 100 W.

3. RESULTS AND DISCUSSION

3.1. Molecular Design. By appropriately sizing the side chains, it is anticipated that the hindrance caused will allow for the locking of specific twisting conformations of the molecular backbone, resulting in unique various molecular packing. In order to support this, we synthesized molecules **1**−**4** (Figure 1) and examined how their twisting conformations in the molecular backbone affected the structures they formed. Molecules **1** and **2** both have longer side chains on the inner fluorene unit and shorter ones on the outer fluorene unit. In contrast, molecule **3** has longer side chains on both fluorene units, whereas molecule **4** has shorter side chains on both fluorene units. The detailed synthesis procedures and characterizations of molecule **1**−**4** are provided in the Supporting Information.

3.2. Formation of 2D Platelets through Heteroseeded Self-Assembly. After the addition of 1 mL of acetonitrile to a chloroform solution containing **1** (0.5 mg/mL, 0.1 mL), and subsequent aging for 24 h, two distinct types of aggregates were formed simultaneously (Figure S9). This is likely attributed to the different backbone twisting of molecule **1**, leading to the distinct morphologies observed. To achieve the specific twisting conformation of molecule **1**, we employed the heteroseeded self-assembly method to guide the epitaxial growth of **1** on seeds, ultimately leading to a singular crystalline structure (Figure S10). Following the addition of different quantities (0.1, 0.04, 0.02, and 0.01 mL) of heteroseeds created from molecule **2** (0.05 mg/mL) in acetonitrile to 1 mL of the supersaturated solution of **1** (0.01 mg/mL) in a blend of chloroform/acetonitrile (v/v, 1/10) in a 4 mL vial, the resulting mixtures were allowed to age at 25 °C for 30 min. Fluorescence optical microscopy revealed that uniform orange-emissive diamond-shaped 2D platelets were formed, with their sizes depending on the molecule-to-seed mass ratios (Figure 2a and Figure S11). SEM confirmed the smooth surface of the 2D platelets (Figure 2b), which was further validated by AFM (Figure 2c). Moreover, the resulting orange-emitting 2D platelets have a narrow area dispersity (Aw/An ≤ 1.02; see Figure 2a and Figure S11). Further analysis revealed a linear relationship between the sizes of the 2D platelets formed and the molecule-to-seed mass ratios (Figure S11e), the characteristic of living seeded self-assembly. SAED analysis confirmed that the orange-emitting 2D platelets are single-crystal structures (Figure S12). To gain deeper insight into the molecular configuration and organization of **1** in the 2D platelets, we carried out SCXRD analysis. As summarized in Table S1, the 2D platelets obtained are classified under the *I*2/*c* monoclinic space group. As shown in Figure 2d, the benzothiadiazole unit and its neighboring fluorene units are nearly coplanar and show minimal twisting. However, this plane is significantly twisted relative to the fluorene units attached on both ends (Figure 2d). Due to the local molecular twisting, the intermolecular distances were measured to be 4.2 and 4.8 Å along the *a*-axis and *b*-axis, respectively (Figure S13). The distances exceed the threshold for π-coupling, indicating that the intermolecular interactions would have minimal impact on the optical properties of the 2D platelets formed, akin to other twisting D−A molecules.[23,32−34] Despite this, the optical characterizations revealed that the absorption and fluorescence spectra of the diamond-shaped 2D platelets were notably red-shifted by 41 and 61 nm (Figure 2e), respectively,

https://doi.org/10.1021/acs.chemmater.4c03183
Chem. Mater. 2025, 37, 1570−1577

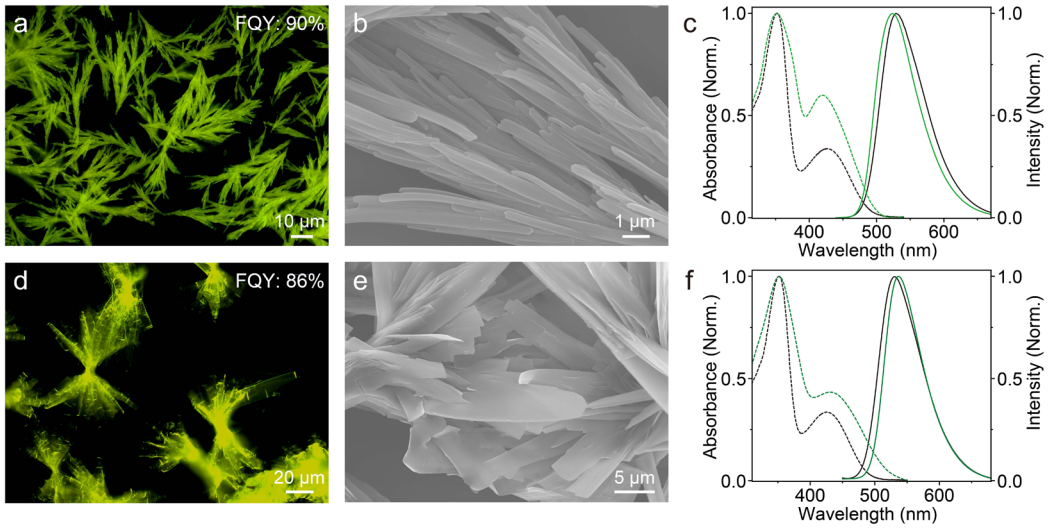

Figure 4. (a) Fluorescence-mode optical image of the aggregates of **3** using the heteroseeding method. (b) SEM image of the aggregates of **3**. (c) UV−vis absorption (dashed) and fluorescence spectra (solid) of molecule **3** (6 μM) in toluene (black) and the aggregates of **3** drop-cast on a glass slide (green). (d) Fluorescence-mode optical images of the aggregates of **4** using the heteroseeding method. (e) SEM image of the aggregates of **4**. (f) UV−vis absorption (dashed) and fluorescence spectra (solid) of molecule **4** (6 μM) in toluene (black) and the aggregates of **4** drop-cast on a glass slide (dark green).

suggesting considerably improved electron coupling. Furthermore, the FQY stayed remarkably high at around 73% (Figure 2a and Table S2). This is in stark contrast to typical supramolecular aggregates, which tend to exhibit reduced emission efficiency alongside a red-shifted fluorescence.[35−38] The local planar structure of molecule **1**, with its benzothiadiazole unit and neighboring fluorene units almost in the same plane, is responsible for increased molecular conjugation, leading to a notable redshift in the optical spectra compared to molecule **1** in toluene solution. Theoretical calculations confirmed a reduced energetic gap of the conformation of molecule **1** (Figure S14), which is consistent with the optical spectra shown in Figure 2e. It is worth noting that the orange-emitting 2D platelets exhibited a longer fluorescence lifetime (τ = 7.92 ns), compared to molecule **1** in toluene solution (τ = 3.02 ns) (see Figure S15 and Table S2). The extended lifetime can be credited to the local molecular planarization of **1** within 2D platelets, which led to excited-state delocalization and ultimately contributed to the increase in lifetime.[39,40] Meanwhile, the twisting between the local plane and the next fluorene attached contributes to the high FQY by minimizing the intermolecular interactions. Put another way, the rates of radiative and nonradiative decay can be altered by the local molecular planarization of **1** within 2D platelets compared to monomer **1** (Table S2). The decreased radiative decay rate (k_r) leads to an increased fluorescence lifetime of 2D platelets compared to monomer **1**, while the slightly increased nonradiative decay rate (k_{nr}) contributes to the decreased fluorescence quantum yield of the 2D platelets.

Notably, the local molecular planarization of **1**, with its benzothiadiazole unit and neighboring fluorene units almost in the same plane formed within 2D platelets, is in stark contrast to all conformers of **2** with large twisting angles between its benzothiadiazole unit and neighboring fluorene units.[15] The increasing steric hindrance from the bulky side chains in molecule **2** likely hinders the generation of the conformer with its benzothiadiazole unit and neighboring fluorene units in a small twisting angle. Similar steric hindrance was also noticed with molecule **3**, as discussed below. Overall, the findings above offer a promising strategy for creating single crystals with significantly red-shifted emission while maintaining high emission efficiency, a desirable quality for optoelectronic applications.

3.3. Formation of the Green-Emitting 1D Microribbons. Interestingly, the orange-emitting 2D platelets formed using heteroseeds are not stable to maintain their form in solution, gradually transitioning into green-emitting 1D microribbons emerge after 8 days (Figure S16). Of note, employing seeded self-assembly allowed for the quick formation of the green-emitting 1D microribbons with controlled sizes (Figure 3a and Figures S10 and S17). SEM and AFM demonstrated the morphology of the 1D microribbons (Figure 3b,c). SAED analysis verified that the green-emitting 1D microribbons are of a single-crystal nature (Figure S18). The morphological shift from 2D platelets to 1D microribbons might be ascribed to molecule **1** adopting more stable packing of twisting conformations. To verify this, we performed SCXRD analysis of the green-emitting crystal. As shown in Table S3, the 1D microribbons obtained are classified under the *P*-1 triclinic space group. Figure 3d shows that molecule **1** in the green-emitting crystal displays two different molecular conformations, each with noticeable twisting between the D and A units. Furthermore, the two twisted conformers were intertwined with each other through electrostatic attraction and hydrophobic interactions, filling up vacant spaces to form a dense structure (Figure 3d). The powder XRD analysis confirmed the high crystallinity of the green-emitting microribbons, as evidenced by multiple well-defined diffraction peaks (Figure S19a). This is in stark contrast to the orange-emitting 2D platelets mentioned earlier, which showed weak diffraction patterns (Figure S19b). Due to the strong molecular packing, the 1D microribbons were able to maintain their structure without alteration for several months (Figure S20).

Apart from the creation of the stable green-emitting 1D microribbons of **1**, the twisted conformations were able to minimize both the intramolecular conjugations and the π-

https://doi.org/10.1021/acs.chemmater.4c03183
Chem. Mater. 2025, 37, 1570−1577

interactions between adjacent molecules. As a result, the optical spectra of the green-emitting microribbons show only a slight shift compared to isolated molecules in solution (Figure 3e). Consequently, the green-emitting microribbons exhibit a high emission efficiency of approximately 87% (Table S2) and a fluorescence lifetime (τ = 3.36 ns) close to that of molecule **1** in toluene (τ = 3.02 ns) (Figure S15 and Table S2). These results clearly demonstrate that a single D−A molecule with a D−D−A−D−D backbone structure and proper side chains can adopt lockable multiple twisting backbone conformations, leading to the formation of diverse crystalline structures with exceptional optical properties.

3.4. Effect of Side Chains on the Presence of Lockable Multiple Backbone Conformations. To delve deeper into how side chains impact the existence of lockable multiple backbone conformations, we compared the self-assembly behaviors of molecules **3** under identical conditions. Utilizing either the heteroseeding approach or the conventional self-assembly method, we obtained the same type of aggregate structure, i.e., the green-emitting aggregates, as illustrated in Figure 4a and Figure S21. SEM imaging revealed a microribbon-like morphology (Figure 4b). These microribbons remained unchanged in shape for an extended period of several months. The absorption and fluorescence spectra of the microribbons of **3** were found to be similar to those of individual **3** in toluene (Figure 4c), suggesting minimal electronic interaction between neighboring **3** molecules. The high FQY of approximately 90% further supports the lack of significant electronic coupling. Upon closer examination, it was found that the absorption and fluorescence spectra of the microribbons composed of **3** were slightly blue-shifted in comparison to those of individual **3** in toluene. This indicates a significant reduction in conjugation, likely because molecule **3** in the microribbons underwent more twisting as a result of the increasing steric hindrance from the bulky side chains. The conjugation reduction of **3** in microribbons is further evidenced by the fact that the microribbons of **3** exhibited a shorter fluorescence lifetime (τ = 2.43 ns) compared to that of molecule **3** in toluene (τ = 3.03 ns) (Figure S22a and Table S2).

Similarly, molecule **4** also formed green-emitting aggregates when utilizing either the heteroseeding approach or the conventional self-assembly method (Figure 4d and Figure S23), despite having very short side chains on the fluorene units. These green-emitting aggregates also took on the form of microribbons (Figure 4e) and remained unchanged for several months. However, they were much wider than those formed from **3**. Interestingly, the absorption and fluorescence spectra and fluorescence lifetime of the microribbons of **4** were found to be comparable to those of individual **4** in solution (Figure 4f, Figure S22b, and Table S2). These results, along with the high FQY of approximately 86%, indicate that there is minimal electronic interaction between neighboring molecules of **4**. This also suggests that molecule **4** adopts a twisting backbone conformation within the microribbons comparable to that in solution.

Based on the above observations, the absence of lockable multiple twisting backbone conformations in molecules **3** is probably due to the presence of long side chains with significant steric hindrance, restricting the twisting flexibility. On the other hand, molecule **4** has minimal steric hindrance, allowing for the formation of the most stable conformation without locking other twisting possibilities. The significant differences in the molecular packing in the aggregates of **3** or **4** and in the seeds of **2**, as evidenced by XRD and SAED analysis in Figure S24, make the aggregation of **3** or **4** unable to be guided by the heteroseeds of **2**. These findings underscore the significance of suitable side-chain lengths in providing the steric hindrance essential for locking multiple twisting conformations of the D−D−A−D−D molecular backbone, ultimately resulting in the emergence of distinct structures and properties.

4. CONCLUSIONS

In summary, we have successfully created the D−A molecule **1** with a D−D−A−D−D backbone structure and appropriate side-chain lengths, enabling the locking of various twisting conformations in the molecular backbone. The application of heteroseeded self-assembly results in the production of orange-emitting 2D platelets. Crystallographic analysis shows that molecule **1** adopts a conformation in which the benzothiadiazole group and its neighboring fluorene groups are almost coplanar but have a considerable twisting angle (around 30°) relative to the next attached fluorene groups. The unique molecular conformation results in 2D platelets exhibiting a noticeable redshift in optical properties compared to molecule **1** in toluene and a high FQY of approximately 73%. Moreover, molecule **1** can form more stable green-emitting 1D microribbons by adopting two intertwined conformations, each with significant twisting angles between the D and A units. These conformations lead to slightly red-shifted optical spectra and a high FQY of around 87%. The findings of this study show that utilizing multiple molecular backbone conformations is an effective strategy for creating distinct crystalline structures with unique properties, while also simplifying the synthesis process by eliminating the need for complex functional groups to control crystalline structures.

■ ASSOCIATED CONTENT

Supporting Information

The Supporting Information is available free of charge at https://pubs.acs.org/doi/10.1021/acs.chemmater.4c03183.

Synthesis of molecules **1**−**4**, ^{1}H NMR and MALDI-MS of molecules **1**−**4**, additional property characterizations of various aggregates, including fluorescence-mode optical microscopic images, XRD and TEM characterizations, etc (PDF)

Single-crystal X-ray diffraction analysis of the orange-emitting 2D platelet of **1** (CIF)

Single-crystal X-ray diffraction analysis of the green-emitting 1D microribbon of **1** (CIF)

■ AUTHOR INFORMATION

Corresponding Authors

Ling Zang − *Department of Material Science and Engineering, University of Utah, Salt Lake City, Utah 84112, United States;* orcid.org/0000-0002-4299-0992; Email: lzang@eng.utah.edu

Yanke Che − *Key Laboratory of Photochemistry, CAS Research/Education Center for Excellence in Molecular Sciences, Institute of Chemistry, Chinese Academy of Sciences, Beijing 100190, China; University of Chinese Academy of Sciences, Beijing 100049, China;* orcid.org/0000-0002-9671-3704; Email: ykche@iccas.ac.cn

https://doi.org/10.1021/acs.chemmater.4c03183
Chem. Mater. 2025, 37, 1570−1577

Authors

Lishan Sun − *Key Laboratory of Photochemistry, CAS Research/Education Center for Excellence in Molecular Sciences, Institute of Chemistry, Chinese Academy of Sciences, Beijing 100190, China; University of Chinese Academy of Sciences, Beijing 100049, China*

Chenglong Liao − *Key Laboratory of Photochemistry, CAS Research/Education Center for Excellence in Molecular Sciences, Institute of Chemistry, Chinese Academy of Sciences, Beijing 100190, China; University of Chinese Academy of Sciences, Beijing 100049, China*

Zihua Zhu − *Key Laboratory of Photochemistry, CAS Research/Education Center for Excellence in Molecular Sciences, Institute of Chemistry, Chinese Academy of Sciences, Beijing 100190, China; University of Chinese Academy of Sciences, Beijing 100049, China*

Yangyang Ren − *Key Laboratory of Photochemistry, CAS Research/Education Center for Excellence in Molecular Sciences, Institute of Chemistry, Chinese Academy of Sciences, Beijing 100190, China; University of Chinese Academy of Sciences, Beijing 100049, China*

Ran Duan − *Key Laboratory of Photochemistry, CAS Research/Education Center for Excellence in Molecular Sciences, Institute of Chemistry, Chinese Academy of Sciences, Beijing 100190, China; University of Chinese Academy of Sciences, Beijing 100049, China*

Hongwei Ji − *Key Laboratory of Photochemistry, CAS Research/Education Center for Excellence in Molecular Sciences, Institute of Chemistry, Chinese Academy of Sciences, Beijing 100190, China; University of Chinese Academy of Sciences, Beijing 100049, China*

Jincai Zhao − *Key Laboratory of Photochemistry, CAS Research/Education Center for Excellence in Molecular Sciences, Institute of Chemistry, Chinese Academy of Sciences, Beijing 100190, China; University of Chinese Academy of Sciences, Beijing 100049, China;* orcid.org/0000-0003-1449-4235

Complete contact information is available at: https://pubs.acs.org/10.1021/acs.chemmater.4c03183

Author Contributions

[+]L.S. and C.L. contributed equally to this work.

Notes

The authors declare no competing financial interest.

■ ACKNOWLEDGMENTS

This work was funded by the National Key Research and Development Program of China (Nos. 2022YFA1205501 and 2019YFA0210401), NSFC (Nos. 21925604 and 22321004), and the Strategic Priority Research Program of Chinese Academy of Sciences (Grant No. XDB36000000).

■ REFERENCES

(1) Lv, Q.; Wang, X. D.; Yu, Y.; Xu, C. F.; Yu, Y. J.; Xia, X. Y.; Zheng, M.; Liao, L. S. Lateral epitaxial growth of two-dimensional organic heterostructures. *Nat. Chem.* **2024**, *16* (2), 201−209.

(2) Lv, Q.; Wang, X.-D.; Yang, W.-Y.; Wang, K.-L.; Xu, C.-F.; Zheng, M.; Liao, L.-S. A General Synthetic Approach of Organic Lateral Heterostructures for Optical Signal Converters in All-Color Wavelength. *CCS Chem.* **2023**, *5* (2), 423−433.

(3) Lv, Q.; Wang, X. D.; Yu, Y.; Zhuo, M. P.; Zheng, M.; Liao, L. S. Lattice-mismatch-free growth of organic heterostructure nanowires from cocrystals to alloys. *Nat. Commun.* **2022**, *13* (1), 3099.

(4) Ogi, S.; Takamatsu, A.; Matsumoto, K.; Hasegawa, S.; Yamaguchi, S. Biomimetic Design of a Robustly Stabilized Folded State Enabling Seed-Initiated Supramolecular Polymerization under Microfluidic Mixing. *Angew. Chem., Int. Ed.* **2023**, *62* (34), No. e202306428.

(5) Fukaya, N.; Ogi, S.; Sotome, H.; Fujimoto, K. J.; Yanai, T.; Bäumer, N.; Fernández, G.; Miyasaka, H.; Yamaguchi, S. Impact of Hydrophobic/Hydrophilic Balance on Aggregation Pathways, Morphologies, and Excited-State Dynamics of Amphiphilic Diketopyrrolopyrrole Dyes in Aqueous Media. *J. Am. Chem. Soc.* **2022**, *144* (49), 22479−22492.

(6) Ogi, S.; Stepanenko, V.; Thein, J.; Würthner, F. Impact of Alkyl Spacer Length on Aggregation Pathways in Kinetically Controlled Supramolecular Polymerization. *J. Am. Chem. Soc.* **2016**, *138* (2), 670−678.

(7) Ogi, S.; Sugiyasu, K.; Manna, S.; Samitsu, S.; Takeuchi, M. Living supramolecular polymerization realized through a biomimetic approach. *Nat. Chem.* **2014**, *6* (3), 188−195.

(8) Fukui, T.; Kawai, S.; Fujinuma, S.; Matsushita, Y.; Yasuda, T.; Sakurai, T.; Seki, S.; Takeuchi, M.; Sugiyasu, K. Control over differentiation of a metastable supramolecular assembly in one and two dimensions. *Nat. Chem.* **2017**, *9* (5), 493−499.

(9) Li, Z.; Xiao, K.; Wan, Q.; Tang, R.; Low, K. H.; Cui, X.; Che, C. M. Controlled Self-assembly of Gold(I) Complexes by Multiple Kinetic Aggregation States with Nonlinear Optical and Waveguide Properties. *Angew. Chem., Int. Ed.* **2023**, *62* (10), No. e202216523.

(10) Wan, Q.; To, W.-P.; Chang, X.; Che, C.-M. Controlled Synthesis of PdII and PtII Supramolecular Copolymer with Sequential Multiblock and Amplified Phosphorescence. *Chem.* **2020**, *6* (4), 945−967.

(11) Zhao, Y.; Kawano, H.; Yamagishi, H.; Otake, S.; Itoh, Y.; Huang, H.; Meijer, E. W.; Aida, T. Pathway Complexity in Nanotubular Supramolecular Polymerization: Metal−Organic Nanotubes with a Planar-Chiral Monomer. *J. Am. Chem. Soc.* **2023**, *145* (25), 13920−13928.

(12) Su, H.; Jansen, S. A. H.; Schnitzer, T.; Weyandt, E.; Rosch, A. T.; Liu, J.; Vantomme, G.; Meijer, E. W. Unraveling the Complexity of Supramolecular Copolymerization Dictated by Triazine-Benzene Interactions. *J. Am. Chem. Soc.* **2021**, *143* (41), 17128−17135.

(13) Suda, N.; Saito, T.; Arima, H.; Yagai, S. Photo-modulation of supramolecular polymorphism in the self-assembly of a scissor-shaped azobenzene dyad into nanotoroids and fibers. *Chem. Sci.* **2022**, *13* (11), 3249−3255.

(14) Suzuki, A.; Aratsu, K.; Datta, S.; Shimizu, N.; Takagi, H.; Haruki, R.; Adachi, S. I.; Hollamby, M.; Silly, F.; Yagai, S. Topological Impact on the Kinetic Stability of Supramolecular Polymers. *J. Am. Chem. Soc.* **2019**, *141* (33), 13196−13202.

(15) Liao, C.; Gong, Y.; Che, Y.; Cui, L.; Liu, Y.; Ji, H.; Zhang, Y.; Zang, L.; Zhao, J.; Che, Y. Living Self-Assembly of Metastable and Stable Two-Dimensional Platelets from a Single Small Molecule. *Chem. − Eur. J.* **2023**, *29* (72), No. e202301747.

(16) Laishram, R.; Sarkar, S.; Seth, I.; Khatun, N.; Aswal, V. K.; Maitra, U.; George, S. J. Secondary Nucleation-Triggered Physical Cross-Links and Tunable Stiffness in Seeded Supramolecular Hydrogels. *J. Am. Chem. Soc.* **2022**, *144* (25), 11306−11315.

(17) Sarkar, S.; Sarkar, A.; Som, A.; Agasti, S. S.; George, S. J. Stereoselective Primary and Secondary Nucleation Events in Multicomponent Seeded Supramolecular Polymerization. *J. Am. Chem. Soc.* **2021**, *143* (30), 11777−11787.

(18) Khanra, P.; Singh, A. K.; Roy, L.; Das, A. Pathway Complexity in Supramolecular Copolymerization and Blocky Star Copolymers by a Hetero-Seeding Effect. *J. Am. Chem. Soc.* **2023**, *145* (9), 5270−5284.

(19) Veedu, R. M.; Niemeyer, N.; Bäumer, N.; Kalathil, K. K.; Neugebauer, J.; Fernández, G. Sterically Allowed H-type Supramolecular Polymerizations. *Angew. Chem., Int. Ed.* **2023**, *62* (49), No. e202314211.

(20) Helmers, I.; Ghosh, G.; Albuquerque, R. Q.; Fernández, G. Pathway and Length Control of Supramolecular Polymers in Aqueous

Media via a Hydrogen Bonding Lock. *Angew. Chem., Int. Ed.* **2021**, *60* (8), 4368−4376.
(21) Matern, J.; Dorca, Y.; Sánchez, L.; Fernández, G. Revising Complex Supramolecular Polymerization under Kinetic and Thermodynamic Control. *Angew. Chem., Int. Ed.* **2019**, *58* (47), 16730−16740.
(22) Sevim, S.; Sorrenti, A.; Franco, C.; Furukawa, S.; Pané, S.; deMello, A. J.; Puigmartí-Luis, J. Self-assembled materials and supramolecular chemistry within microfluidic environments: from common thermodynamic states to non-equilibrium structures. *Chem. Soc. Rev.* **2018**, *47* (11), 3788−3803.
(23) Gong, Y.; Cheng, C.; Ji, H.; Che, Y.; Zang, L.; Zhao, J.; Zhang, Y. Unprecedented Small Molecule-Based Uniform Two-Dimensional Platelets with Tailorable Shapes and Sizes. *J. Am. Chem. Soc.* **2022**, *144* (33), 15403−15410.
(24) Fu, L.; Che, Y.; Gong, Y.; Ji, H.; Zhang, Y.; Zang, L.; Zhao, J.; Che, Y. Control over the Geometric Shapes and Mechanical Properties of Uniform Platelets via Tunable Two-Dimensional Living Self-Assembly. *Chem. Mater.* **2023**, *35* (3), 1310−1317.
(25) Tong, Z.; Xie, Y.; Arno, M. C.; Zhang, Y.; Manners, I.; O'Reilly, R. K.; Dove, A. P. Uniform segmented platelet micelles with compositionally distinct and selectively degradable cores. *Nat. Chem.* **2023**, *15* (6), 824−831.
(26) MacFarlane, L. R.; Shaikh, H.; Garcia-Hernandez, J. D.; Vespa, M.; Fukui, T.; Manners, I. Functional nanoparticles through π-conjugated polymer self-assembly. *Nat. Rev. Mater.* **2021**, *6* (1), 7−26.
(27) He, X.; Hsiao, M. S.; Boott, C. E.; Harniman, R. L.; Nazemi, A.; Li, X.; Winnik, M. A.; Manners, I. Two-dimensional assemblies from crystallizable homopolymers with charged termini. *Nat. Mater.* **2017**, *16* (4), 481−488.
(28) Kotha, S.; Sahu, R.; Yadav, A. C.; Sharma, P.; Kumar, B. V. V. S. P.; Reddy, S. K.; Rao, K. V. Noncovalent synthesis of homo and hetero-architectures of supramolecular polymers via secondary nucleation. *Nat. Commun.* **2024**, *15* (1), 3672.
(29) Liao, C.; Gong, Y.; Che, Y.; Ji, H.; Liu, B.; Zang, L.; Che, Y.; Zhao, J. Concentric hollow multi-hexagonal platelets from a small molecule. *Nat. Commun.* **2024**, *15* (1), 5668.
(30) Ren, Y.; Gong, Y.; Che, Y.; Liao, C.; Ji, H.; Cui, L.; Zang, L.; Che, Y.; Zhao, J. Seeded Growth of Three-Dimensional Block Heterojunctions Featuring Photoinduced Emission Enhancement. *Chem. Mater.* **2024**, *36* (13), 6567−6574.
(31) Liu, Y.; Gong, Y.; Guo, Y.; Xiong, W.; Zhang, Y.; Zhao, J.; Che, Y.; Manners, I. Emergent Self-Assembly Pathways to Multidimensional Hierarchical Assemblies using a Hetero-Seeding Approach. *Chem. − Eur. J.* **2019**, *25* (59), 13484−13490.
(32) Cui, L.; Gong, Y.; Yu, X.; Lv, C.; Du, X.; Zhao, J.; Che, Y. Development of a Fluorophore with Enhanced Unorthodox Chalcogen Bonding for Highly Sensitive Detection of Trimethyl Arsine Vapor. *ACS Sens.* **2021**, *6* (8), 2851−2857.
(33) Feng, Z.; Li, Y.; Chen, S.; Li, J.; Wu, T.; Ying, Y.; Zheng, J.; Zhang, Y.; Zhang, J.; Fan, X.; et al. Engineered NIR-II fluorophores with ultralong-distance molecular packing for high-contrast deep lesion identification. *Nat. Commun.* **2023**, *14* (1), 5017.
(34) Shen, H.; Sun, F.; Zhu, X.; Zhang, J.; Ou, X.; Zhang, J.; Xu, C.; Sung, H. H. Y.; Williams, I. D.; Chen, S.; et al. Rational Design of NIR-II AIEgens with Ultrahigh Quantum Yields for Photo- and Chemiluminescence Imaging. *J. Am. Chem. Soc.* **2022**, *144* (33), 15391−15402.
(35) Zhang, H.; Zhao, Z.; Turley, A. T.; Wang, L.; McGonigal, P. R.; Tu, Y.; Li, Y.; Wang, Z.; Kwok, R. T. K.; Lam, J. W. Y.; et al. Aggregate Science: From Structures to Properties. *Adv. Mater.* **2020**, *32* (36), No. e2001457.
(36) Wagner, W.; Wehner, M.; Stepanenko, V.; Ogi, S.; Wurthner, F. Living Supramolecular Polymerization of a Perylene Bisimide Dye into Fluorescent J-Aggregates. *Angew. Chem., Int. Ed.* **2017**, *56* (50), 16008−16012.
(37) Würthner, F.; Saha-Möller, C. R.; Fimmel, B.; Ogi, S.; Leowanawat, P.; Schmidt, D. Perylene Bisimide Dye Assemblies as Archetype Functional Supramolecular Materials. *Chem. Rev.* **2016**, *116* (3), 962−1052.
(38) Ma, X.; Zhang, Y.; Zhang, Y.; Peng, C.; Che, Y.; Zhao, J. Stepwise Formation of Photoconductive Nanotubes through a New Top-Down Method. *Adv. Mater.* **2015**, *27* (47), 7746−7751.
(39) Takada, T.; Ashida, A.; Nakamura, M.; Fujitsuka, M.; Majima, T.; Yamana, K. Photocurrent generation enhanced by charge delocalization over stacked perylenediimide chromophores assembled within DNA. *J. Am. Chem. Soc.* **2014**, *136* (19), 6814−6817.
(40) Hollinbeck, S. R.; Liu, K.; Olivier, J.-H.; Grumstrup, E. M. Probing Excited State Delocalization and Charge Separation in Hierarchical Perylene Diimide Materials with Time-Resolved Broadband Microscopy. *J. Phys. Chem. C* **2024**, *128* (19), 7977−7986.

https://doi.org/10.1021/acs.chemmater.4c03183
Chem. Mater. 2025, 37, 1570−1577